Structure of *N*-Acetylproline Amide in Liquid Water: Experimentally Measured and Numerically Simulated Infrared and Vibrational Circular Dichroism Spectra†

Kyung-Koo Lee,‡ Seungsoo Hahn,‡ Kwang-Im Oh,‡ Jin Seok Choi,§ Cheonik Joo,§ Hochan Lee,‡ Hogyu Han,§ and Minhaeng Cho*,‡

Department of Chemistry and Center for Multidimensional Spectroscopy, Division of Chemistry and Molecular Engineering, Korea University, Seoul 136-701, Korea, and Department of Chemistry, Division of Chemistry and Molecular Engineering, Korea University, Seoul 136-701, Korea

Received: October 13, 2005; In Final Form: February 19, 2006

A few experimental and theoretical studies on the molecular structure of *N*-acetylproline amide (AP) in D_2O solution have been reported recently. However, there is no consensus of the precise structure of AP in D_2O because spectroscopically determined structures and a theoretically simulated one have been found to be different from one another. To determine its aqueous solution structure, IR and vibrational circular dichroism spectra of both L- and D-form AP solutions were measured. Molecular dynamics simulations with two different force fields and density functional theory calculations for the trans and cis rotamers of AP were performed to numerically simulate those spectra. Comparisons between experimentally measured and computationally simulated spectra directly suggest that the AP in water adopts a polyproline II-like conformation and that the force field parameter *ff*03 in the AMBER 8 suite of programs is more realistic and reliable in predicting molecular structure of AP in water than the *ff*99 in AMBER 7.

I. Introduction

A variety of vibrational spectroscopies such as IR absorption, Raman scattering, vibrational circular dichroism, and Raman optical activity spectroscopies have been extensively used to determine secondary structures of polypeptides in solutions.[1−4] Among different polypeptide vibrational degrees of freedom, the amide I band in the frequency range from 1600 to 1700 cm^{-1} has been paid a great deal of attention because its position and line shape are known to be very sensitive to the secondary structure of a given polypeptide.[5−7]

Recently, two-dimensional (2D) vibrational spectroscopies employing heterodyne-detected IR photon echo or frequency-dispersed pump−probe methods have been used to extract vital information on three-dimensional (3D) structure of small oligopeptides in solutions.[8−14] For instance, Woutersen and Hamm[15] obtained the 2D IR pump−probe spectra of trialanine (H_2N-$(Ala)_3$-COOH) and their isotopomers, and they concluded that the dominant conformation of the trialanine in liquid water is the polyproline II (P_{II}) form. Schweitzer-Stenner et al. studied triproline[16a] and poly-L-proline[16b] in D_2O and found that they adopt a P_{II} structure. Eker et al.[17,18] showed that the structure of Ac-L-Ala-L-Ala-OH is a mixture of P_{II} and β-strand conformations by using the combined IR and nonresonant Raman spectroscopic studies. In addition, Hochstrasser and co-workers performed a 2D IR photon echo experiment on the alanine dipeptide, Ac-Ala-NHMe, in liquid water and reached a conclusion that the P_{II} conformation is the most probable structure,[19] and the result is consistent with the liquid crystal NMR spectroscopic one obtained by Poon et al.[20]

Although the conformation of *alanine-based* short peptides has been found to be P_{II}, several molecular dynamics (MD) simulation packages currently available unfortunately predict quite different structures for small oligopeptides. For instance, Hermans and co-workers[21] carried out a series of classical MD simulations of capped alanine dipeptide in liquid water by using six different force fields implemented in the available computer simulation programs. They found that, for such a small peptide system, the ensemble averaged conformation greatly depends on which set of force field parameters is used. For instance, one of the most popular simulation package AMBER with force field parameter *ff*94, developed by Cornell et al.,[22] predicted that the global energy minimum conformation of the alanine dipeptide in TIP3P water potential is close to the right-handed α-helix, α_R. On the other hand, other programs such as GROMOS or CHARMM suggest that the dipeptide can adopt two different conformers, P_{II} and α_R, though the relative populations predicted by these simulation packages differ from each other. On the basis of this and related simulation studies, it is believed that the classical MD force fields should be further refined to be of use in structure determination of small oligopeptides in water.[23]

Although the alanine dipeptide can be considered to be an ideal prototype peptide system for a variety of experimental and theoretical simulation studies, an alternative peptide system that is useful for detailed investigations can be the *N*-acetylproline amide (AP).[24−27] The free amine of a proline amino acid is blocked with an acetyl group, and its carboxyl group is changed into an amide in AP (see Figure 1). One can assign two amide I local modes to the acetyl- and amide-end peptide bonds. Depending on the conformation of the acetyl group with respect to the pyrrolidine ring, there exist two conformational isomers denoted as *trans*-AP and *cis*-AP, respectively. The potential energy barrier between the *trans*-AP and *cis*-AP is relatively large so that we could not find any conformational

† Part of the special issue "Robert J. Silbey Festschrift".

* To whom correspondence should be addressed. E-mail: mcho@korea.ac.kr.

‡ Department of Chemistry and Center for Multidimensional Spectroscopy.

§ Department of Chemistry.

10.1021/jp055846+ CCC: $33.50
Published on Web 03/29/2006

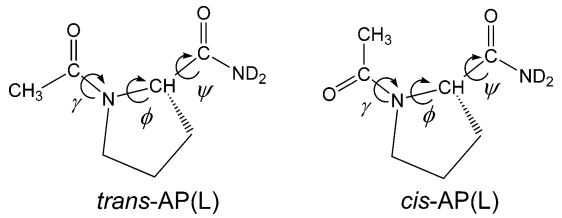

Figure 1. Chemical structures of the *trans*-AP ($\gamma = 180°$) and *cis*-AP ($\gamma = 0°$) in L-form. Its secondary structure is determined by the two dihedral angles ϕ and ψ. L-Form AP was considered for all theoretical calculations unless otherwise noted in Figures 3−8.

transitions between the two isomers during tens of nanoseconds MD simulations; note that the time scale for such conformational transition between *trans*- and *cis*-AP is slow enough to identify the two forms in a typical NMR (nuclear magnetic resonance) spectrum. The solution structures of Ac-Pro-NHMe were studied long ago by Madison and Kopple,[28] and they found that the internally hydrogen-bonded C_7 form predominates in nonpolar solvents, but that extended P_{II} form and α_R coexist in polar solvents. More recently, the AP in solutions was studied by Zanni et al.,[24] Ge et al.,[25] and Rubsov et al.[26] by using the 2D IR photon echo and transient absorption measurement techniques. They suggested that the predominant conformation of AP in nonpolar solvent such as CH_2Cl_2 is C_7 structure, which is consistent with the previous observation. However, the ensemble average conformation of AP in water was suggested to be neither P_{II} nor α_R because their estimated angle between the transition dipoles of the two amide I modes was found to be less than 20° (see ref 24 for detailed discussions on this point). Later, Ge et al. found that there are two conformations of AP in D_2O.[25]

To quantitatively simulate both the 1D and 2D vibrational spectra of AP in liquid water and chloroform, we carried out molecular dynamics simulations in combination with extensive density functional theory (DFT) calculations of gas-phase *trans*-AP.[29] Once the amide I local mode frequencies, vibrational coupling constant, dipole strength, and rotational strength are obtained as functions of the two dihedral angles ϕ and ψ, one can numerically simulate both IR and vibrational circular dichroism (VCD) spectra. MD simulation method was used to calculate the dipole−dipole correlation function associated with the IR absorption spectrum and the amide I mode frequency−frequency correlation function required in calculations of linear and nonlinear vibrational response functions. The force field and program used in ref 29 was *ff*99[30] and AMBER 7,[31] respectively, with TIP3P water potential. We found that the predominant conformations of *trans*-AP in liquids $CDCl_3$ and D_2O are close to C_7 and α_R (or 3_{10}-helix), respectively. Despite that the AP structure in nonpolar solvent predicted by that simulation study appeared to be in good agreement with previous experimental observation;[26,28] here it should be noted that the experimental studies were performed for AP and Ac-Pro-NHMe in refs 26 and 28, respectively, it was found that the predicted AP structure in D_2O is notably different from the structures suggested earlier by other workers.[28] Therefore, still it is not clear which AP conformer predominates in an aqueous solution. Furthermore, the question on which force field and MD simulation package are suitable for structure determination of small oligopeptides in water has not been fully addressed yet.

Consequently, the principle goal of the present work is twofold. The first one is to determine 3D structure of AP in liquid water by directly comparing experimentally measured IR and VCD spectra with theoretically predicted (numerically simulated) ones. Second, we will show that, in the case of AP in water, the *ff*03[32] in AMBER 8[33] is more reliable than the *ff*99 in AMBER 7. In Section II, experimental methods for the preparation and spectral measurement of L- and D-form AP's are briefly outlined. Density functional theory calculation and MD simulation results will be discussed in Section III. Theoretical descriptions of IR and VCD spectroscopies for the conformationally inhomogeneous dipeptide system and results and discussions will be presented in Sections IV and V, respectively. The main results and a few concluding comments will be given in Section VI.

II. Materials and Methods

Ac-L-Pro-NH_2 (L-AP). To a stirred solution of L-proline amide (H-L-Pro-NH_2, 2.0 g, 17.5 mmol, Novabiochem) in dry CH_2Cl_2 (20 mL) was added *N*,*N*-diisopropylethylamine (9.16 mL, 52.6 mmol) and then acetic anhydride (4.95 mL, 52.5 mmol) at 0 °C. After stirring at room temperature for 14 h, the reaction mixture was concentrated at 25 °C in vacuo. The precipitate was filtered, washed with cold CH_2Cl_2, and dried in vacuo to give the title compound (1.72 g, 63%) as a white solid. TLC ($MeOH/CH_2Cl_2 = 1:9$) $R_f = 0.36$; ^1H NMR (500 MHz, D_2O) two rotamers at 25 °C (3.1:1), major rotamer δ 4.38 (dd, $J = 8.5$, 4.0 Hz, 1H), 3.71−3.61 (m, 2H), 2.35−2.26 (m, 1H), 2.13 (s, 3H), 2.04−1.97 (m, 3H), minor rotamer δ 4.54 (dd, $J = 8.5$, 3.0 Hz, 1H), 3.59−3.48 (m, 2H), 2.43−2.35 (m, 1H), 2.16−2.10 (m, 1H), 2.03 (s, 3H), 2.02−1.86 (m, 2H); ^{13}C NMR (125 MHz, D_2O) major rotamer δ 180.21, 176.04, 62.71, 51.50, 32.94, 27.00, 24.24, minor rotamer δ 180.09, 176.25, 64.26, 49.88, 34.55, 25.35, 24.05; HRMS (EI+) for $C_7H_{12}N_2O_2$ (M^+), calcd 156.0899, found 156.0900.

Ac-D-Pro-NH_2 (D-AP). To a stirred solution of D-proline amide (H-D-Pro-NH_2, 500 mg, 4.38 mmol, Novabiochem) in dry CH_2Cl_2 (6 mL) was added *N*,*N*-diisopropylethylamine (2.29 mL, 13.1 mmol) and then acetic anhydride (1.24 mL, 13.1 mmol) at 0 °C. After stirring at room temperature for 14 h, the reaction mixture was concentrated at 25 °C in vacuo. The precipitate was filtered, washed with cold CH_2Cl_2, and dried in vacuo to give the title compound (520 mg, 76%) as a white solid. TLC ($MeOH/CH_2Cl_2 = 1:9$) $R_f = 0.32$; ^1H NMR (500 MHz, D_2O) two rotamers at 25 °C (3.1:1), major rotamer δ 4.38 (dd, $J = 8.8$, 3.8 Hz, 1H), 3.71−3.61 (m, 2H), 2.35−2.26 (m, 1H), 2.14 (s, 3H), 2.04−1.98 (m, 3H), minor rotamer δ 4.54 (dd, $J = 8.8$, 3.3 Hz, 1H), 3.60−3.48 (m, 2H), 2.43−2.36 (m, 1H), 2.16−2.11 (m, 1H), 2.03 (s, 3H), 2.02−1.86 (m, 2H); ^{13}C NMR (125 MHz, D_2O) major rotamer δ 180.21, 176.04, 62.70, 51.50, 32.94, 27.00, 24.23, minor rotamer δ 180.09, 176.26, 64.26, 49.88, 34.55, 25.34, 24.05; HRMS (EI+) for $C_7H_{12}N_2O_2$ (M^+), calcd 156.0899, found 156.0898.

IR and VCD Spectroscopy. IR and VCD spectra were measured with a Chiral*ir* FT-VCD spectrometer from Bomem/BioTools. This spectrometer is equipped with a HgCdTe detector having a cutoff at 8 cm^{-1} and a ZeSe photoelastic modulator (PEM) to create left and right circularly polarized radiation. The PEM was optimized for maximum quarter-wave response at 1400 cm^{-1}. To exchange the labile hydrogen atoms in AP to deuterium atoms, the peptide/D_2O solution was lyophilized twice on a SpeedVac (ThermoSavant), and subsequently, it was dissolved in D_2O to a concentration of 50 mg/mL. VCD and IR spectra were measured in D_2O with resolution of 4 cm^{-1} by using a CaF_2 cell with a path length of 25 μm, and the sample cell chamber was purged with dehydrated N_2 gas. Temperature of the sample cell was controlled by a circulating water bath (Sam Heung Instrument SH-R-WB10), and a temperature

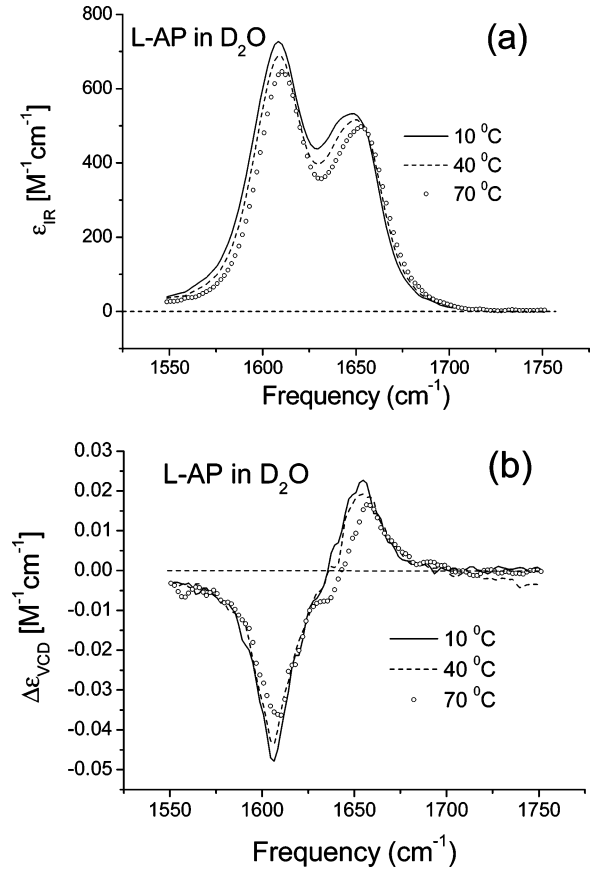

Figure 2. Experimentally measured IR (a) and VCD (b) spectra of 50 mg/mL L-AP in water (D_2O) for varying temperature from 10 to 70 °C. See experimental details in Section II.

sensor was directly attached to the cell surface. VCD spectra were collected in blocks for a total collection time of approximately 12 h (32688 AC scans and 600 DC scans collected in 12 blocks) depending on the peptide sample investigated. The VCD baseline correction was made with both D- and L-AP spectra separately measured (Figure 2).

NMR Spectroscopy. For the determination of the trans/cis ratio for AP at various temperatures in D_2O, ^1H NMR experiments were carried out on a Bruker Avance 500 NMR spectrometer. The trans/cis ratio was determined by analyzing the integration ratio of major to minor rotamer signals of H_α at δ 4.38 and δ 4.54, respectively. The trans/cis ratio decreased with increasing temperature for both L-AP and D-AP (10 mg/mL AP in D_2O, 10 °C, trans/cis = 3.3:1; 25 °C, 3.1:1; 40 °C, 3.0:1; 60 °C, 2.6:1). To investigate the possible dimerization of AP at 25 °C in D_2O, ^1H NMR spectra for AP at various concentrations were recorded on a Varian Mercury 300 NMR spectrometer. ^1H NMR spectra were nearly identical over the L-AP concentration range from 0.01 to 1.0 M, indicating that dimers or higher aggregates were not formed in such a concentration range.

III. Quantum Chemistry Calculations and MD Simulations

A. Density Functional Theory Calculation. To obtain the exciton Hamiltonian matrix elements of the AP trans and cis rotamers, we first carried out density functional theory calculations at the B3LYP/6-311++G** level by using the Gaussian 03 suite.[34] The range of dihedral angle ϕ for a trans (cis) rotamer is restricted between −120 (−110) to −10 (−30) and that of ψ is from −100 (−180) to 180 (180). For a given AP configuration with fixed angles ϕ and ψ, both geometry optimization and vibrational analysis were performed.

From the amide I normal mode frequencies and eigenvectors extracted from the DFT vibrational analyses, we could identify the two amide I local modes, which are largely localized on either acetyl-end or amide-end peptide bonds, and estimate vibrational coupling constants by using the extended Hessian matrix reconstruction (EHMR) method.[12,35] In Figure 3, these local mode frequencies and coupling constants for both *trans*- and *cis*-AP in a gas phase are plotted. Here, the excitonic coupling constants of P_{II} and 3_{10}-helix conformations for *trans*-AP (*cis*-AP) are 4.4 (3.7) and 0.9 (1.7) cm^{-1}, respectively. The electric and magnetic transition dipole moments of the two normal modes were also determined (not shown). For both *trans*- and *cis*-AP, the amide-end amide I local mode frequency is found to be larger than the acetyl-end one. However, because of the relative distance and orientation of the acetyl-end peptide bond with respect to the amide-end peptide bond, the vibrational properties of *cis*-AP are quite different from those of *trans*-AP, as can be seen in Figure 3. For numerical simulations of IR and VCD spectra, we will directly use these data though the ensemble averaged conformations of both *trans*- and *cis*-AP will be determined with an MD simulation method.

As mentioned in the Introduction, the stable conformation of Ac-Pro-NHMe in nonpolar solvent has been known to be the C_7 structure that is stabilized by an intramolecular hydrogen-bonding interaction.[28] In Figure 4a, the potential energy surface of *trans*-AP in a gas phase is plotted as a function of ϕ and ψ. Within the B3LYP/6-311++G** approximation, indeed, the global minimum conformation of *trans*-AP is predicted to be C_7. However, for the *cis*-AP, the minimum energy conformation is between C_7 and right-handed α-helix (Figure 4b). Thus, to determine the global minimum conformation of AP, one needs to know the relative population of trans rotamer with respect to that of cis rotamer in condensed phase and to carry out detailed quantum chemistry calculations. On the basis of DFT-calculated potential energy surfaces of the *trans*-AP and *cis*-AP, it is clear that the energy minimum conformations of these two rotamers are quite different from the extended structures such as β-sheets or P_{II} when it is in a gas phase or dissolved in nonpolar solvents.

B. MD Simulation Method. To study hydration effects on the molecular structure of AP, we newly carried out several different MD simulations. By using the LEaP module,[33] we prepared two different structures of AP, i.e., trans and cis forms. Equilibrium MD simulation for *trans*-AP (*cis*-AP) was run for 2 ns (2.5 ns). The force field parameter set of *ff*03 was used for these simulations. The system consists of a single *trans*-AP (*cis*-AP) molecule and 740 (794) TIP3P D_2O molecules. A periodic boundary condition was employed. Each system was equilibrated for a few nanoseconds at 298 K by using the Berendsen coupling algorithm[36] in a constant temperature condition to make the density to be 1.107 g/cm^3 and for additional 1 ns in a constant volume condition to make the system relaxed in a new constraint.

We found that the conformational transitions of both *trans*-AP and *cis*-AP from a 3_{10}-helical conformer to a P_{II}-like conformer rarely occur during a few nanoseconds of simulation at 298 K. Therefore, we carried out high-temperature MD simulations with either explicit or implicit solvents. Thus obtained conformational search results were found to be strongly dependent on the force field used in the MD simulation. Here, we used two different parameter sets, *ff*99 and *ff*03, implemented in the AMBER 7 and AMBER 8 suites of programs, respectively.

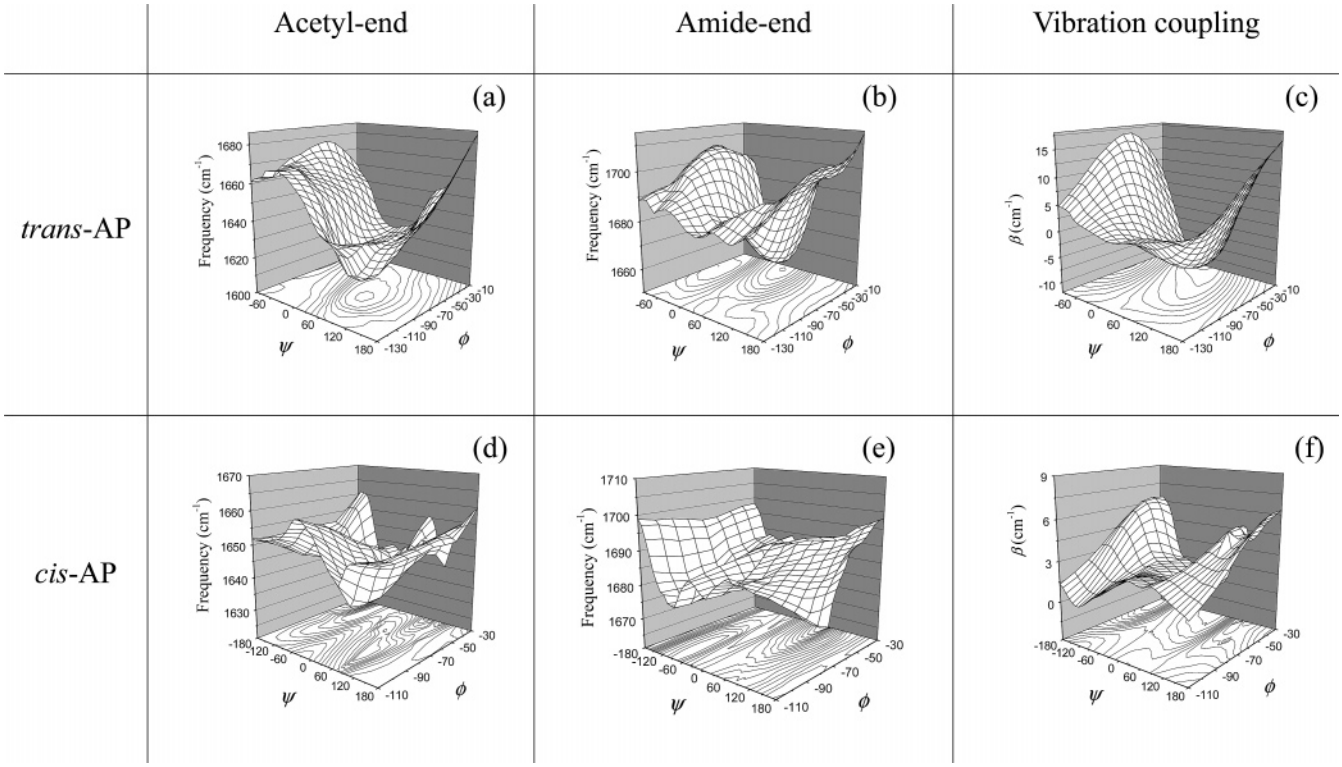

Figure 3. Two amide I local mode frequencies of the acetyl- and amide-end peptides and the vibrational coupling constants plotted with respect to ϕ and ψ for both *trans*- and *cis*-AP in a gas phase.

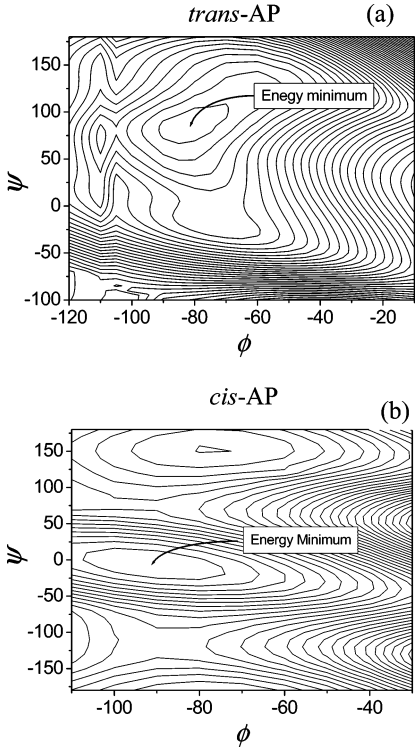

Figure 4. Potential energy surfaces of isolated *trans*-AP (a) and *cis*-AP (b) molecules in a gas phase. The energy minimum conformation for *trans*-AP is predicted to be C_7, whereas that for *cis*-AP is between C_7 and α_R.

The high-temperature MD simulations were performed for 10 ns at 500 K by using the pressure coupling algorithm in a constant temperature condition with explicit TIP3P water solvent. Furthermore, we also conducted 100 ns MD simulations at 500 K by using a modified generalized Born solvation model[37] to examine whether there exist any other structural transitions that could not be sampled by the 10 ns 500 K MD simulation with explicit water solvent. For these two different high-temperature simulations, both *ff*99 and *ff*03 force fields were employed to further investigate the force-field-dependence of the ensemble-averaged structure of AP in water.

C. Conformational Analysis of AP in D_2O Solution. From the 10 ns explicit solvent MD trajectory at 500 K, the distributions of the two dihedral angles ϕ and ψ for both rotamers were obtained and plotted in Figure 5. As can be seen in Figure 5a and b, the *ff*99 force field suggests that the predominant conformations of *trans*- and *cis*-AP molecules in water are predicted to be close to 3_{10}-helix. In strong contrast, the *ff*03 force field predicts that the most stable conformation of AP is close to the P_{II} structure for both *trans*- and *cis*-AP. Because in ref 29 we used *ff*99 force field in the MD simulations of *trans*-AP in water, the *trans*-AP structure was assumed to be 3_{10}-helix II ($\phi \approx -74$, $\psi \approx -4$). Subsequently, we calculated IR, VCD, and 2D IR spectra based on the *ff*99 simulation results. However, in the present work, it is shown that the *ff*99 force field prediction on the 3D structure of AP in water significantly differs from the *ff*03 prediction. More specifically, *trans*-AP adopts major P_{II}- and minor 3_{10}-helix-like conformers with average dihedral angles of ($\phi = -69$, $\psi = 155$) and ($\phi = -71$, $\psi = -19$), respectively. Similarly, *cis*-AP also adopts major P_{II}- and minor 3_{10} helix-like conformers and have average dihedral angles of ($\phi = -72$, $\psi = 159$) and ($\phi = -74$, $\psi = -23$), respectively. Note that the average ϕ and ψ angles when the AP is either P_{II}-like or 3_{10}-helix-like do not depend on the precise conformation of the acetyl group.

Later in this paper, we will show which force field provides results that are consistent with experimental findings. Although we have not presented detailed analysis results on 100 ns 500 K MD simulations with *ff*03 and implicit (modified generalized Born solvation (GBS)) solvent model, the ϕ and ψ distributions obtained from this GBS simulations are found to be very similar to Figure 5c and d. From Figure 5c and 5d, for both *trans*- and

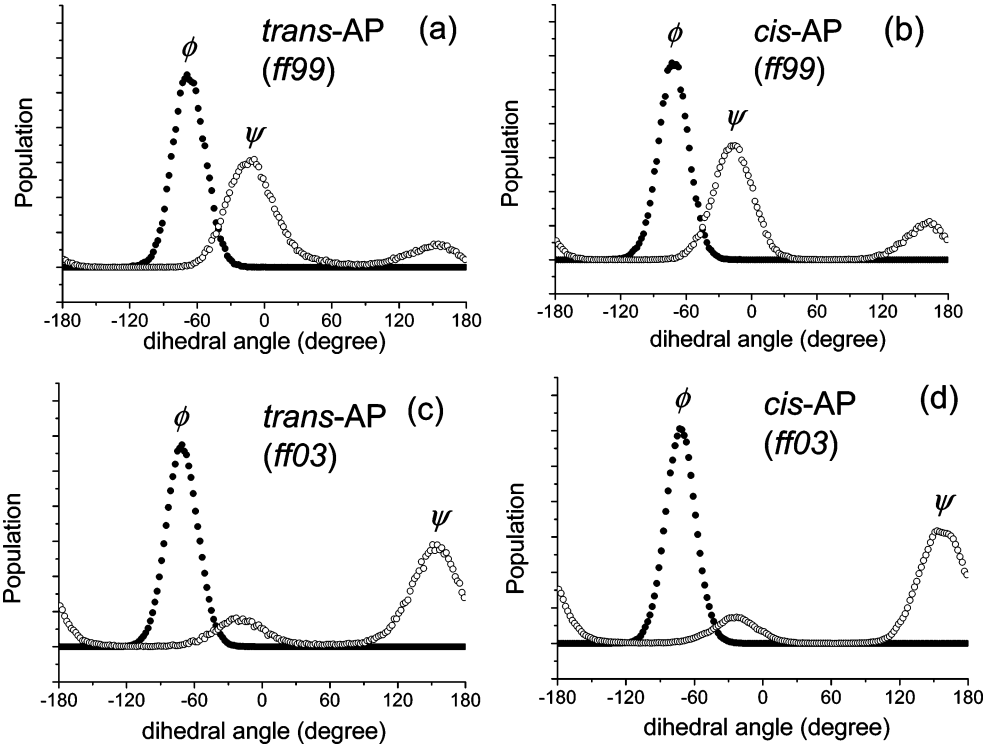

Figure 5. Population distributions of ϕ and ψ angles for *trans*- and *cis*-AP molecules in liquid water. Here, we used the 10 ns 500 K MD simulation (with explicit TIP3P water potential) results. The upper two figures (a) and (b) are obtained from the *ff*99 force field simulation (with AMBER 7), whereas the lower two figures (c) and (d) are from the *ff*03 force field simulation (AMBER 8). The conformation of AP in (a) and (b) is close to 3_{10}-helix, whereas that in (c) and (d) is close to P_{II}.

cis-AP, we find that the ratio of P_{II}-like population to 3_{10}-helix-like population is about 4:1 at 500 K. Then, using the single histogram (SH) equation,[38] one can find that the ratio of P_{II} to 3_{10}-helix population is 9:1 at room temperature for both *trans*- and *cis*-AP in liquid water. We will next use these two sets of MD trajectories for *trans*- and *cis*-AP aqueous solutions to numerically simulate the corresponding IR and VCD spectra, and they will be directly compared with experiments in Section V.

IV. Numerical Simulations of IR and VCD Spectra

As discussed in detail in ref 29, one can use the correlation function formalism to numerically simulate the IR and VCD spectra of AP in liquid water. In this section, we will briefly outline the theory and computational procedure. By using the interaction picture, the molecular Hamiltonian, including the system-bath interaction term, can be written as[35]

$$H(t) = H_0 + \delta H(t) \tag{1}$$

where $H(t)$ is the Heisenberg operator defined as $H(t) = \exp(iH_B t/\hbar)H \exp(-iH_B t/\hbar)$ with H_B being the bath Hamiltonian. The zero-order and fluctuating part of the molecular Hamiltonian are given as, respectively,

$$H_0 = |1,0\rangle \hbar\bar{\omega}_{Ac} \langle 1,0| + |0,1\rangle \hbar\bar{\omega}_{Am} \langle 0,1| + |1,0\rangle \hbar\bar{\beta} \langle 0,1| + |0,1\rangle \hbar\bar{\beta} \langle 1,0|$$

$$\delta H(t) = |1,0\rangle \hbar\delta\omega_{Ac}(t) \langle 1,0| + |0,1\rangle \hbar\delta\omega_{Am}(t) \langle 0,1| + \hbar\delta\beta(t)\{|1,0\rangle \langle 0,1| + |0,1\rangle \langle 1,0|\} \tag{2}$$

Here, $|m,n\rangle$ and $\langle m,n|$ denote the ket- and bra-states in which the acetyl-end peptide and the amide-end peptide have m and n vibrational quanta, respectively. The ensemble averaged amide I local mode frequencies of the acetyl- and amide-end peptides and coupling constant are denoted as $\bar{\omega}_{Ac}$, $\bar{\omega}_{Am}$, and $\bar{\beta}$, respectively. The fluctuating amide I local mode frequencies were denoted as $\delta\omega_{Ac}(t)$ and $\delta\omega_{Am}(t)$ in eq 2, and the coupling constant fluctuation $\delta\beta(t)$ in eq 2 is defined as $\delta\beta(t) = \beta(t) - \bar{\beta}$. For a given instantaneous configuration sampled from the MD trajectory, dihedral angles ϕ and ψ can be determined. Then, it is possible to obtain both the diagonal and off-diagonal Hamiltonian matrix elements by using the DFT-calculated local mode frequencies of acetyl- and amide-end peptides as well as the coupling constant for either *trans*- or *cis*-AP molecule in liquid water (see Figure 3). However, still it is necessary to use an empirical frequency correction method to quantitatively take into account the solvation effects on amide I local mode frequencies. In ref 29, such a method was described in detail.

Now, to obtain *normal mode* frequencies and to describe their dynamical fluctuations, the zero-order Hamiltonian H_0 should be diagonalized first, i.e.,

$$H_0' = U^T H_0 U \tag{3}$$

where U is the corresponding eigenvector matrix. Then, we have

$$H_0' = |e_1\rangle \hbar\bar{\omega}_{e_1 g} \langle e_1| + |e_2\rangle \hbar\bar{\omega}_{e_2 g} \langle e_2| \tag{4}$$

where $|e_n\rangle$ (for $n = 1$ and 2) are the two one-exciton states, respectively. The corresponding average transition frequencies were denoted as $\bar{\omega}_{e_n g}$. By using the same orthogonal transformation U-matrix, the fluctuating part of the molecular Hamiltonian, $\delta H(t)$, can be transformed as $\delta H'(t) = U^T \delta H(t) U$ so that the fluctuating transition frequencies of the two normal modes are found to be $\delta\omega_{e_n g}(t) = \langle e_n|U^T \delta H(t) U|e_n\rangle$ (for $n = 1$ and 2). In the present work, we will ignore the residual off-diagonal terms, $\langle e_1|U^T \delta H(t) U|e_2\rangle$ and $\langle e_2|U^T \delta H(t) U|e_1\rangle$, that can induce popula-

tion transfers between the two one-exciton states. Now, the frequency−frequency correlation functions $C_1(t)$ and $C_2(t)$ are defined as

$$C_1(t) = \langle \delta\omega_{e_1g}(t)\delta\omega_{e_1g}(0)\rangle$$
$$C_2(t) = \langle \delta\omega_{e_2g}(t)\delta\omega_{e_2g}(0)\rangle \quad (5)$$

and they will be used to numerically simulate the IR and VCD spectra in the following subsections.

A. IR Spectroscopy. For a mixed solution with both *trans*-AP and *cis*-AP being present at room temperature, the IR absorption spectrum, $I(\omega)$, can be written as, in terms of the linear response function $J(t)$,[39]

$$I(\omega) \sim \mathrm{Re}\int_0^\infty \mathrm{d}t e^{i\omega t - t/2T_1}\sum_{k=1}^{2}\{P_{\mathrm{trans}}D_k^{\mathrm{trans}}\, e^{-i\bar{\omega}_{e_kg}^{\mathrm{trans}}t}J_k^{\mathrm{trans}}(t) + P_{\mathrm{cis}}D_k^{\mathrm{cis}}\, e^{-i\bar{\omega}_{e_kg}^{\mathrm{cis}}t}J_k^{\mathrm{cis}}(t)\} \quad (6)$$

where $\bar{\omega}_{e_kg}^{\mathrm{trans}}$ ($\bar{\omega}_{e_kg}^{\mathrm{cis}}$) is the ensemble averaged kth amide I normal mode transition frequency of the *trans*-AP (*cis*-AP) and the dipole strength D_k^{trans} (D_k^{cis}) is defined as $D_k^{\mathrm{trans/cis}} \equiv |(\partial\mu^{\mathrm{trans/cis}}/\partial Q_k)_0|^2$ for the *trans*-AP (*cis*-AP). The dipole strengths of the two normal modes for *trans*-AP as well as for *cis*-AP are presented in the Supporting Information A. The probability of finding *trans*-AP (*cis*-AP) is denoted as P_{trans} (P_{cis}) and from the NMR spectrum analysis we found that $P_{\mathrm{trans}} = 0.75$ and $P_{\mathrm{cis}} = 0.25$. The vibrational pure dephasing contribution is described by the linear response function $J_k(t)$ defined as

$$J_k(t) \equiv \langle \exp_+[-i\int_0^t \mathrm{d}\tau\delta\omega_{e_kg}(\tau)]\rangle \quad (7)$$

By using a semiclassical approximation, treating the fluctuating frequency as a classical variable, and the second-order cumulant expansion technique, the linear response function $J(t)$ in eq 7 can be expressed in terms of the frequency−frequency correlation function of $\delta\omega_{e_kg}(\tau)$ as,

$$J_k(t) = \exp\{-\int_0^t \mathrm{d}\tau_1\int_0^{\tau_1}\mathrm{d}\tau_2 C_k(\tau_2)\} \quad (8)$$

where $C_k(t)$ were defined in eq 5.

Although the vibrational pure dephasing process was taken into consideration here by using the cumulant expansion approximation,[40] the additional contribution originating from the intrinsic population relaxation of amide I vibrationally excited states has not been considered properly. This lifetime broadening effect is going to be taken into account in an ad hoc manner, and the T_1 constant in eq 6 is assumed to be 0.5 ps.

B. VCD Spectroscopy. For the present case of AP solution, we find that the VCD spectrum can be calculated as[39]

$$\Delta I_{\mathrm{VCD}}(\omega) \sim \mathrm{Re}\int_0^\infty \mathrm{d}t e^{i\omega t - t/2T_1}\sum_{k=1}^{2}\{P_{\mathrm{trans}}R_k^{\mathrm{trans}}\, e^{-i\bar{\omega}_{e_kg}^{\mathrm{trans}}t}J_k^{\mathrm{trans}}(t) + P_{\mathrm{cis}}R_k^{\mathrm{cis}}\, e^{-i\bar{\omega}_{e_kg}^{cis}t}J_k^{\mathrm{cis}}(t)\} \quad (9)$$

where the rotational strength of the kth normal mode is defined as

$$R_k = \mathrm{Im}[(\partial\boldsymbol{\mu}/\partial Q_k)_0\cdot(\partial\mathbf{m}/\partial Q_k)_0] \quad (10)$$

Here, the electric and magnetic dipole moments of the electronic ground-state molecule were denoted as $\boldsymbol{\mu}$ and $\mathbf{m}$, respectively. By using the magnetic field perturbation (MFP) theory,[41,42] the gauge-invariant rotational strength can be calculated with the Gaussian 03 program package. Again, the B3LYP/6-311++G** calculation method was used to evaluate the rotational strengths of the two normal modes of the *trans*-AP and *cis*-AP as a function of ϕ and ψ (detailed contour plots of these rotational strengths for amide I normal modes can be found in the Supporting Information B).

V. Results and Discussions

A. Experimental Observations. In Figure 2a and b, the IR and VCD spectra of L-AP are shown; note that the IR spectrum of D-AP was also measured and found to be indistinguishable from that of L-AP. As expected, the VCD spectrum of L-AP is a mirror image of that of D-AP. The VCD spectra of L-AP in Figure 2b for varying temperature from 10 to 70 °C show two peaks that are associated with the low-frequency acetyl-end amide I mode and the high-frequency amide-end amide I mode. Here, the signs of the two peaks provide critical information on the 3D molecular structure of L-AP in water.

In ref 29, we deliberately considered five representative AP conformations, such as α_R, P_{II}, C_7, 3_{10}-helix I, and 3_{10}-helix II structures of L-form *trans*-AP, and the numerically simulated IR and VCD spectra were presented (see Figure 9a and c in ref 29). The right-handed α-helical AP showed a typical (+,−) couplet in the VCD spectrum. On the other hand, the VCD spectra of C_7, 3_{10}-helix I, and 3_{10}-helix II conformers produce all negative VCD peaks, and only the P_{II} conformation can produce a (−,+) couplet pattern in its VCD spectrum. Thus, comparing the Figure 2b in this paper with the VCD spectrum of model P_{II} conformer in ref 29, one can immediately reach a conclusion that the most populated AP structure in water is P_{II}. However, in ref 29, we did not properly take into account the *cis*-AP contributions to the IR and VCD spectra, and furthermore, the *ff*99 MD simulation result in ref 29 does not appear to be consistent with the present VCD measurement. We will present a detailed discussion along this line in the following subsection.

Before this subsection is closed, a comment on temperature dependence of AP structure in water should be given. The IR and VCD spectra of L-AP in D_2O were collected in the

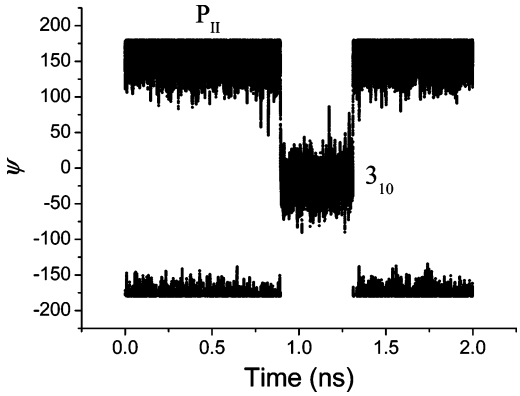

Figure 6. Trajectory of ψ angle extracted from the 2 ns 298 K MD simulation for *trans*-AP with *ff*03 force field and explicit TIP3P water potential. Note that there are conformational transitions between P_{II}-like conformation and 3_{10}-helix-like conformation. The time scale of these conformation transitions is fairly slow at 298 K so that we carried out 500 K MD simulation to speed up the transitions and to cover a wider range of configuration space.

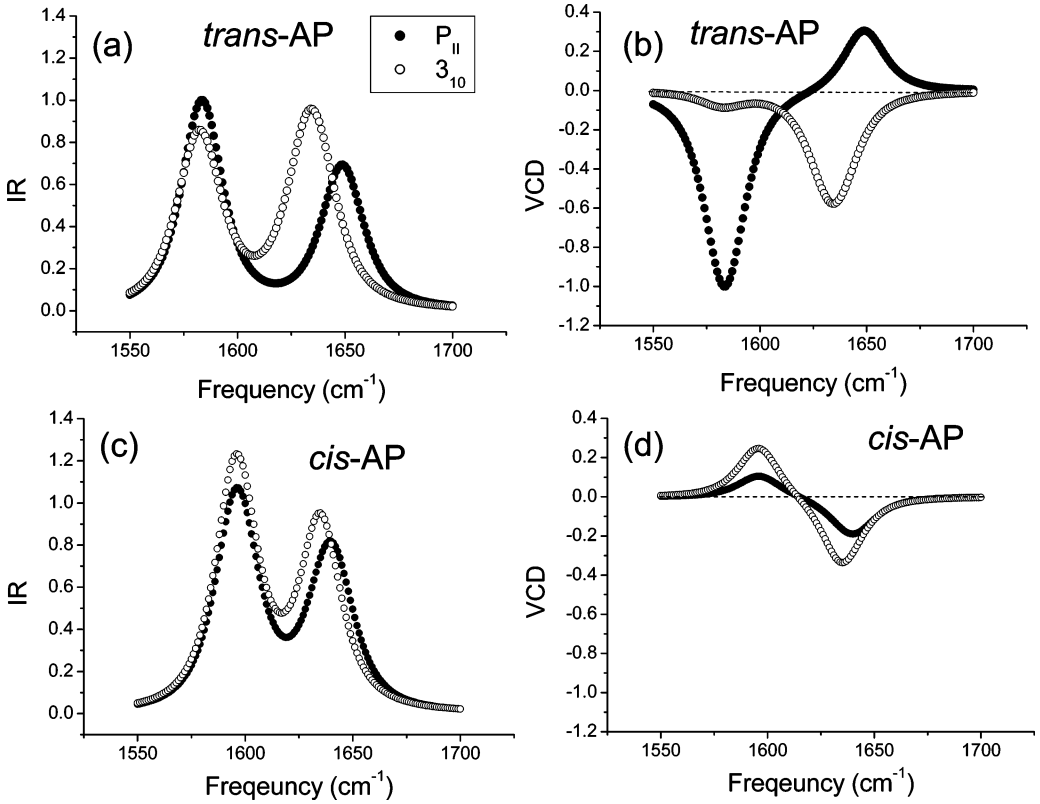

Figure 7. Numerically simulated IR and VCD spectra of P_{II}- and 3_{10}-helix-like *trans*-AP and *cis*-AP molecules in water. We used the 2 ns 298 K MD simulation results shown in Figure 6 to separately calculate these IR and VCD spectra. The solvatochromic amide I mode frequency shift and fluctuation were taken into account by carrying out MD simulations of AP in liquid water and by using the extrapolation method.[29] One should properly multiply weighting factors (trans/cis = 3:1 and $P_{II}/3_{10}$ = 9:1 at 298 K) to these individual spectra to finally calculate the total IR and VCD spectra of L-AP in liquid water shown in Figure 8. The trans/cis ratio could be determined by NMR analysis (Section II), whereas the $P_{II}/3_{10}$ ratio is obtained from the *ff*03 simulation and single histogram method (Section III.C). It is noteworthy that trans−cis and $P_{II}-3_{10}$ are respectively related to dihedral angles γ and $\phi-\psi$ whereby the backbone structures are determined as shown in Figure 1. The ratio between AP backbone conformers is found to be determined by a combination of trans/cis and $P_{II}/3_{10}$ ratios.

temperature range from 10 to 70 °C, and they show little dependence on *T*. As *T* increases from 10 to 70 °C, both peaks in either IR or VCD spectra exhibit slightly blue-shifting behaviors, indicating that the average number of hydrogen-bonded water molecules decreases as *T* increases. Also, it is found that the bandwidths in both IR and VCD spectra increase a little bit. This suggests that the predominant conformation of L-AP in D_2O does not change in this temperature range.

B. Numerically Simulated IR and VCD Spectra. The 2 ns 298 K equilibrium MD simulations for the *trans*-AP solution were used to properly model the amide I mode frequency fluctuations and vibrational dephasing processes at room temperature. In Figure 6, the time-dependent dihedral angle $\psi(t)$ for *trans*-AP is particularly plotted. During this 2 ns simulation, two conformational transitions between P_{II} and 3_{10}-helix occurred. Thus, by following the procedure discussed in ref 29 for *N*-methylacetamide in methanol solution,[43] one can divide the entire phase space into two regions where the conformation of *trans*-AP is either P_{II} or 3_{10}-helix. This means that the response function can be approximately written as a sum of two terms representing the P_{II}- and 3_{10}-helix-form AP molecules,

$$J_k(t) = P_{P_{II}} \exp\{-\int_0^t d\tau_1 \int_0^{\tau_1} d\tau_2 C_k^{P_{II}}(\tau_2)\} + P_{3_{10}} \exp\{-\int_0^t d\tau_1 \int_0^{\tau_1} d\tau_2 C_k^{3_{10}}(\tau_2)\} \quad (11)$$

where the probabilities of finding P_{II} and 3_{10}-helix conformations for a given *trans*-AP or *cis*-AP are denoted as $P_{P_{II}}$ and $P_{3_{10}}$, respectively, and they are $P_{P_{II}} = 0.9$ and $P_{3_{10}} = 0.1$ at room temperature. Now, from the two separated MD trajectories and with eqs 6, 9, and 11, it becomes possible to numerically calculate the associated IR and VCD spectra (or corresponding linear response functions) for the *trans*-AP, which are plotted in Figure 7a and b, respectively. Similarly, the 2.5 ns 298 K equilibrium MD simulation for the *cis*-AP solution was performed, and the corresponding IR and VCD spectra were calculated and plotted in Figure 7c and d (see Appendix for a detailed discussion on the numerical calculation methods). Note that the P_{II} conformation of the *trans*-AP exhibits a typical (−,+) couplet line shape in VCD spectrum (see Figure 7b), whereas the 3_{10}-helix conformation of *cis*-AP shows a (+,−) couplet pattern, which is typical for right-handed helical polypeptides (see Figure 7d). Also, it is interesting to note that the VCD spectrum of the *cis*-AP shows the same (+,−) couplet feature for both P_{II} and 3_{10}, whereas that of *trans*-AP for P_{II} is opposite in sign.

Now, noting that the ratio of *trans*-AP to *cis*-AP population is 3:1 and that the ratio of P_{II} to 3_{10}-helix population in both *trans*-AP and *cis*-AP solutions is 9:1 at room temperature, we could calculate the total IR and VCD spectra and plot them in Figure 8a and b (see the solid curves), respectively. In these figures, the open circles are the experimental data (at 10 °C) in Figure 2. To quantitatively compare the simulated spectra with experimental ones, the maximum (or minimum) peak intensities in both IR and VCD spectra are normalized. In both cases, we find that the low-frequency peak, which is associated with the vibrational transition of the acetyl-end amide I mode, predicted by the present DFT calculations is too much red-shifted by about

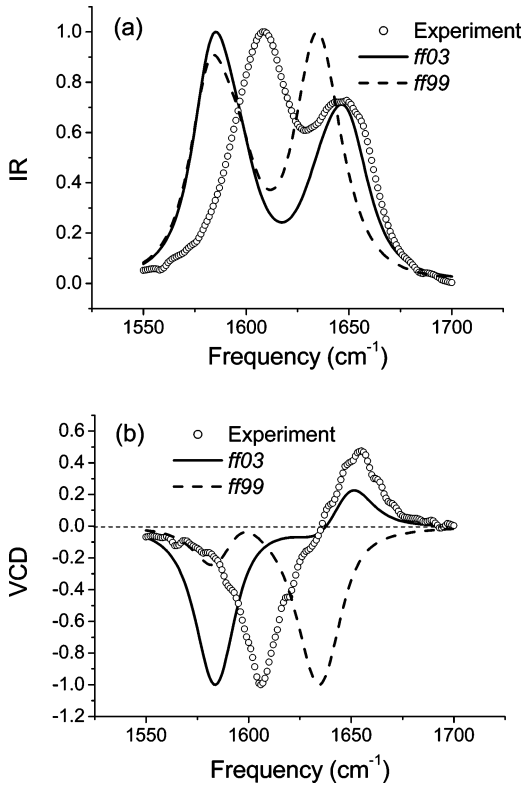

Figure 8. Comparison between experimentally measured IR (a) and VCD (b) spectra at 10 °C (open circles) and numerically simulated ones by using *ff*99 (dashed curves) and *ff*03 (solid curves). For quantitative comparison, both IR and VCD spectra from Figure 2 were normalized. In the cases of *ff*03-simulated spectra, except for ~20 cm^{-1} blue-shifted low-frequency peaks, the overall line shape and intensity distribution of the two peaks in both IR and VCD spectra predicted by the *ff*03 simulation are in good agreement with experiments.

20 cm^{-1}, in comparison to experimentally measured frequency. Despite this frequency mismatch, the overall line shapes and intensity ratios found in the numerically simulated IR and VCD spectra are in excellent agreement with experiments. Here it should be emphasized that, except for the lifetime broadening factor, no adjustable parameters were introduced to theoretically predict the IR and VCD spectra. Thus, it is believed that the present comparative investigation and good agreements found in this work suggest that the computational procedure combining MD simulation with DFT calculations of the gas phase AP molecules can be of use in quantitatively predicting vibrational spectra of small oligopeptides in condensed phases.

Now, it is ready to directly compare the two force fields, *ff*99 and *ff*03, which were implemented in AMBER 7 and AMBER 8 programs. In Figure 8a and b, the numerically simulated IR and VCD spectra (see the dashed curves) by using the AMBER 7 MD simulation results are also plotted and compared with those (solid curves) obtained with the *ff*03 force field as well as with experimental results (open circles). It should be noted that the *ff*99-predicted IR spectrum differs from the *ff*03 result, that is to say, the intensity of the high-frequency peak of the *ff*99-predicted spectrum is much larger than that of the *ff*03 spectrum, and the frequency-splitting amplitude depends on the force field used. Despite that the *ff*03 spectrum appears much more similar to the experimentally measured one, it is clear that the IR absorption spectroscopy itself cannot be the incisive tool for determining the conformation of AP in water nor for examining the validity of force field used. On the contrary, the VCD spectra predicted by *ff*99 and *ff*03 dramatically differ from each other. Clearly, the VCD spectrum numerically simulated by using the AMBER 8 (*ff*03) MD trajectory is much closer to the experimental curve. This indicates that the *ff*03 force field has been successfully improved over the previous version, *ff*99, at least for the present dipeptide system.

C. Comparisons with Other Related Works. Recently, the conformational preference of alanine dipeptide in water has been extensively studied theoretically by using a variety of MD simulation techniques and quantum chemistry calculations. Such computational studies were mainly motivated by recent optical spectroscopic observation suggesting that the dominant alanine dipeptide conformer corresponds to the left-handed P_{II} in water solution. On the basis of extensive quantum chemistry calculations of alanine dipeptide with a few solvating water molecules, it has been recognized that the preference of aqueous alanine dipeptide for P_{II}-like conformer is largely determined by favorable peptide−water hydrogen-bonding interactions, where water bridges are formed between the carbonyl oxygen atom and the nearby amide hydrogen atom.[20,44] However, Drozdov et al. carried out MD simulation studies of alanine dipeptide in water by using parameters from the all-atom OPLS force field and found that the experimentally observed preference of alanine dipeptide in water for P_{II} does not arise due to favorable peptide−water interactions.[45] The determining factor for such conformational preference is a consequence of minimizing intrapeptide steric conflicts. The role of solvent water molecules in this case is to screen the intrapeptide electrostatic (Coulombic) interaction to make the van der Waals and torsional potential the dominant interaction in determining the shape of peptide conformational potential energy surface in water.

In comparison to the alanine dipeptide, the AP does not have an amide hydrogen atom in the acetyl-end peptide due to the presence of a pyrrolidine ring so that one of the two water bridges found in ref 20 is intrinsically not allowed. Second, in the case of *cis*-AP, because of its structural geometry, the carbonyl oxygen atom in the acetyl-end peptide cannot participate in hydrogen-bonding interaction with the other short water bridge connecting carbonyl oxygen atom of the acetyl-end peptide and amide hydrogen atom of the amide-end peptide. Therefore, it is believed that the AP system is an ideal model for addressing the questions: What is the influence of water on peptide geometry? And do the peptide−water interactions through the formation of water bridges between the peptide H-bond donor and acceptor groups play a critical role?

Interestingly, despite the inability of AP to form such specific water bridges with just a few water molecules, the most stable AP conformer for both *trans*- and *cis*-AP is found to be the P_{II}-like one. The present experimental and molecular dynamics simulation (*ff*03) results can thus be considered to be independent supporting evidence that the recent argument provided by Pappu and co-workers[45] on the conformational preference of alanine dipeptide in water can also be used to explain the P_{II}-like conformation of AP in water. That is to say, the peptide−water interaction itself is certainly important, but it may not be the sole determining factor in stabilizing P_{II}-like AP conformer in water, even though the solvation dynamics by water molecules plays a crucial role in vibrational frequency shifts and fluctuations inducing a spectral line broadening.

VI. Summary

As emphasized in the Introduction, there are two principle goals of the present investigation combining experimental measurements of IR and VCD spectra of AP in water with theoretical simulation studies. It is believed that we have

achieved these two goals. First of all, we found that the 3D structure of AP in liquid water is close to an extended (left-handed helical) P_{II}-like conformation. Second, the improved force field parameter *ff*03 implemented in the AMBER 8 suite is superior to the *ff*99 force field because the numerically simulated IR and VCD spectra of AP in water by using the *ff*03 force field simulation are in good agreement with experimental results. Currently, we are studying other polar and nonpolar solvent effects on the 3D structure of dipeptide and carrying out a series of MD simulations to address the issue on the specific peptide−solvent interaction effects on polypeptide structures in condensed phases. It is believed that the present computational algorithm combining quantum chemistry calculation and properly chosen MD simulation methods can be of use in studying polypeptide structures in solutions.

Appendix

Three Different Computational Methods of IR and VCD Spectra. There are a few different ways to numerically simulate IR and VCD spectra from the MD trajectory. In this appendix, we will compare three calculation schemes that differ from one another by how to use the MD-simulated coordination files.

Method 1. From the MD trajectory, one can determine ensemble average structure of the dipeptide. That is to say, the ensemble average ϕ and ψ angles, $\langle\phi\rangle$ and $\langle\psi\rangle$, are determined first. The amide I local mode frequencies, coupling constant, transition electric dipole, transition magnetic dipole, and average solvatochromic frequency shifts for that ensemble average conformation are determined and used to construct the zero-order Hamiltonian in eq 2. The remaining computational procedure was already described in the main text.

Method 2. Instead of taking the ensemble average conformation of AP in water, one can directly calculate the ensemble average amide I local mode frequencies, $\bar{\omega}_{Ac}$ and $\bar{\omega}_{Am}$, and coupling constant $\bar{\beta}$. The residual fluctuating parts of local mode frequencies and coupling constant, due to the solvation dynamics and conformational fluctuation of AP in water, are taken into account for describing dephasing processes.

Method 3. The above two methods are common in nature because they both require a reference zero-order Hamiltonian. In contrast, one can use the instantaneous normal mode (INM) approach to numerically simulating IR and VCD spectra. From the MD trajectory, we first sampled thousands of instantaneous configurations. From each instantaneous conformation of AP and by using the contour maps of local mode frequencies, coupling constant, and transition electric and magnetic dipoles, one can obtain thousands of IR and VCD spectra, where each spectral line was assumed to be a Lorentzian function and broadened by the intrinsic lifetime broadening factor, $T_1 = 0.5$ ps. Then, the final IR and VCD spectra are obtained by taking the ensemble average spectra over the thousands of IR and VCD spectra.

In Figure 9a and b, the IR and VCD spectra calculated by using these three different methods are plotted. The spectra obtained from the ensemble average AP conformations (method 1) are indistinguishable from those from the ensemble average frequencies and coupling constant (method 2). On the other hand, the INM-calculated spectra (method 3) are found to be significantly broader than the other two spectra.[11,46] This is because the INM analysis is, strictly speaking, corresponding to the static inhomogeneous line-broadening limit. That is to say, the motional narrowing effect induced by the ultrafast solvent dynamics was not correctly taken into consideration in the INM approach to the vibrational spectrum simulation. The spectra in Figures 7 and 8 were obtained by using the second method 2 above.

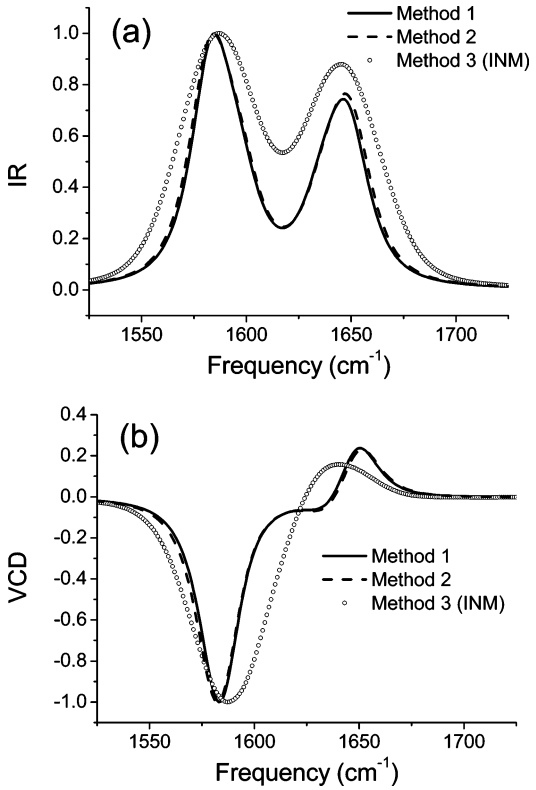

Figure 9. Numerically simulated IR and VCD spectra by using three different methods discussed in Appendix.

Acknowledgment. M.C. is thankful for financial support through the CRI program of KISTEP (MOST, Korea). Also, this work was supported by the Basic Research (grant no. R01-2003-000-11623-0 to H.H.) and CRM programs from KOSEF. Fellowship from the BK21 program (J.S.C. and C.J.) is gratefully acknowledged.

Supporting Information Available: Dipole strengths defined for the two normal modes of *trans*- and *cis*-AP in a gas phase (A); rotational strengths defined for the two normal modes of *trans*- and *cis*-AP in a gas phase (B). This material is available free of charge via the Internet at http://pubs.acs.org.

References and Notes

(1) *Infrared Spectroscopy of Biomolecules*; Mantsch, H. H., Chapman, D., Eds.; Wiley-Liss: New York, 1996.
(2) *Infrared and Raman Spectroscopy of Biological Materials*; Gremlich, H.-U., Yan, B., Eds.; Marcel Dekker: New York, 2000.
(3) Surewicz, W. K.; Mantsch, H. H. In *Spectroscopic Methods for Determining Protein Structure in Solution*; Havel, H. A., Ed.; VCH: New York, 1996; p 135.
(4) Nafie, L. A.; Freedman, T. B. In *Circular Dichroism: Principles and Applications*; Berova, N., Nakanishi, K., Woody, R. W., Eds.; Wiley-Liss: New York, 2000; p 97.
(5) Krimm, S.; Bandekar, J. *Adv. Protein Chem.* **1986**, *38*, 181.
(6) Susi, H.; Byler, D. M. *Arch. Biochem. Biophys.* **1987**, *258*, 465.
(7) Surewicz, W. K.; Mantsch, H. H. *Biochim. Biophys. Acta* **1988**, *952*, 115.
(8) Woutersen, S.; Hamm, P. *J. Phys.: Condens. Matter* **2002**, *14*, R1035.
(9) Khalil, M.; Demirdöven, N.; Tokmakoff, A. *J. Phys. Chem. A* **2003**, *107*, 5258.
(10) Mukamel, S. *Annu. Rev. Phys. Chem.* **2000**, *51*, 691.
(11) Ham, S.; Hahn, S.; Lee, C.; Kim, T.-K.; Kwak, K.; Cho, M. *J. Phys. Chem. B* **2004**, *108*, 9333.
(12) Choi, J.-H.; Hahn, S.; Cho, M. *Int. J. Quantum Chem.* **2005**, *104*, 616.

(13) Hahn, S.; Kim, S.; Lee, C.; Cho, M. *J. Chem. Phys.* **2005**, *123*, 084905.

(14) Wang, J.; Hochstrasser, R. M. *Chem. Phys.* **2004**, *297*, 195.

(15) Woutersen, S.; Hamm, P. *J. Chem. Phys.* **2000**, *114*, 2727.

(16) (a) Schweitzer-Stenner, R.; Eker, F.; Perez, A.; Griebenow, K.; Cao, X.; Nafie, L. A. *Biopolymers* **2003**, *71*, 558. (b) Measey, T.; Schweitzer-Stenner, R. *Chem. Phys. Lett.* **2005**, *408*, 123.

(17) Eker, F.; Cao, X.; Nafie, L.; Schweitzer-Stenner, R. *J. Am. Chem. Soc.* **2002**, *124*, 14330.

(18) Eker, F.; Griebenow, K.; Schweitzer-Stenner, R. *J. Am. Chem. Soc.* **2003**, *125*, 8178.

(19) Kim, Y. S.; Wang, J.; Hochstrasser, R. M. *J. Phys. Chem. B* **2005**, *109*, 7511.

(20) Poon, C.-D.; Samulski, E. T.; Weise, C. F.; Weisshaar, J. C. *J. Am. Chem. Soc.* **2000**, *122*, 5642.

(21) Hu, H.; Elstner, M.; Hermans, J. *Proteins* **2003**, *50*, 451.

(22) Cornell, W. D.; Cieplak, P.; Bayly, C. I.; Gould, I. R.; Merz, K. M.; Ferguson, D. M.; Spellmeyer, D. C., Jr.; Fox, T.; Caldwell, J. W.; Kollman, P. A. *J. Am. Chem. Soc.* **1995**, *117*, 5179.

(23) Ponder, J. W.; Case, D. A. *Adv. Protein Chem.* **2003**, *66*, 27.

(24) Zanni, M. T.; Gnanakaran, S.; Stenger, J.; Hochstrasser, R. M. *J. Phys. Chem. B* **2001**, *105*, 6520.

(25) Ge, N.-H.; Zanni, M. T.; Hochstrasser, R. M. *J. Phys. Chem. A* **2002**, *106*, 962.

(26) Rubtsov, I. V.; Hochstrasser, R. M. *J. Phys. Chem. B* **2002**, *106*, 9165.

(27) Ge, N. H.; Hochstrasser, R. M. *PhysChemComm* **2002**, *5*, 17.

(28) Madison, V.; Kopple, K. D. *J. Am. Chem. Soc.* **1980**, *102*, 4855.

(29) Hahn, S.; Lee, H.; Cho, M. *J. Chem. Phys.* **2004**, *121*, 1849.

(30) Wang, J.; Cieplak, P.; Kollman, P. A. *J. Comput. Chem.* **2000**, *21*, 1049.

(31) Case, D. A.; Pearlman, D. A.; Caldwell, J. W.; Cheatham, T. E., III; Wang, J.; Ross, W. S.; Simmerling, C. L.; Darden, T. A.; Merz, K. M.; Stanton, R. V.; Cheng, A. L.; Vincent, J. J.; Crowley, M.; Tsui, V.; Gohlke, H.; Radmer, R. J.; Duan, Y.; Pitera, J.; Massova, I.; Seibel, G. L.; Singh, U. C.; Weiner, P. K.; Kollman, P. A. *AMBER 7*; University of California: San Francisco, 2002.

(32) Duan, Y.; Wu, C.; Chowdhury, S.; Lee, M. C.; Xiong, G.; Zhang, W.; Yang, R.; Cieplak, P.; Luo, R.; Lee, T. *J. Comput. Chem.* **2003**, *24*, 1999.

(33) Case, D. A.; Darden, T. A.; Cheatham, T. E., III; Simmerling, C. L.; Wang, J.; Duke, R. E.; Luo, R.; Merz, K. M.; Wang, B.; Pearlman, D. A.; Crowley, M.; Brozell, S.; Tsui, V.; Gohlke, H.; Mongan, J.; Hornak, V.; Cui, G.; Beroza, P.; Schafmeister, C.; Caldwell, J. W.; Ross, W. S.; Kollman, P. A. *AMBER 8*; University of California: San Francisco, 2004.

(34) Frisch, M. J.; Trucks, G. W.; Schlegel, H. B.; Scuseria, G. E.; Robb, M. A.; Cheeseman, J. R.; Montgomery, J. A., Jr.; Vreven, T.; Kudin, K. N.; Burant, J. C.; Millam, J. M.; Iyengar, S. S.; Tomasi, J.; Barone, V.; Mennucci, B.; Cossi, M.; Scalmani, G.; Rega, N.; Petersson, G. A.; Nakatsuji, H.; Hada, M.; Ehara, M.; Toyota, K.; Fukuda, R.; Hasegawa, J.; Ishida, M.; Nakajima, T.; Honda, Y.; Kitao, O.; Nakai, H.; Klene, M.; Li, X.; Knox, J. E.; Hratchian, H. P.; Cross, J. B.; Bakken, V.; Adamo, C.; Jaramillo, J.; Gomperts, R.; Stratmann, R. E.; Yazyev, O.; Austin, A. J.; Cammi, R.; Pomelli, C.; Ochterski, J. W.; Ayala, P. Y.; Morokuma, K.; Voth, G. A.; Salvador, P.; Dannenberg, J. J.; Zakrzewski, V. G.; Dapprich, S.; Daniels, A. D.; Strain, M. C.; Farkas, O.; Malick, D. K.; Rabuck, A. D.; Raghavachari, K.; Foresman, J. B.; Ortiz, J. V.; Cui, Q.; Baboul, A. G.; Clifford, S.; Cioslowski, J.; Stefanov, B. B.; Liu, G.; Liashenko, A.; Piskorz, P.; Komaromi, I.; Martin, R. L.; Fox, D. J.; Keith, T.; Al-Laham, M. A.; Peng, C. Y.; Nanayakkara, A.; Challacombe, M.; Gill, P. M. W.; Johnson, B.; Chen, W.; Wong, M. W.; Gonzalez, C.; Pople, J. A. *Gaussian 03*, revision C.02; Gaussian, Inc.: Wallingford, CT, 2004.

(35) Hahn, S.; Ham, S.; Cho, M. *J. Phys. Chem. B* **2005**, *109*, 11789.

(36) Berendsen, H. J. C.; Postma, J. P. M.; van Gunsteren, W. F.; DiNola, A.; Haak, J. R. *J. Chem. Phys.* **1984**, *81*, 3684.

(37) Onufriev, A.; Bashford, D.; Case, D. A. *J. Phys. Chem. B* **2000**, *104*, 3712.

(38) Salsburg, Z. W.; Jacobson, J. D.; Fickett, W.; Wood, W. W. *J. Chem. Phys.* **1959**, *30*, 65.

(39) Kwac, K.; Cho, M. *J. Chem. Phys.* **2003**, *119*, 2247.

(40) Mukamel, S. In *Principles of Nonlinear Optical Spectroscopy*; Oxford University Press: New York, 1995.

(41) Stephens, P. J. *J. Phys. Chem.* **1985**, *89*, 748.

(42) Cheeseman, J. R.; Frisch, M. J.; Devlin, F. J.; Stephens, P. J. *Chem. Phys. Lett.* **1996**, *252*, 211.

(43) Kwac, K.; Lee, H.; Cho, M. *J. Chem. Phys.* **2004**, *120*, 1477.

(44) Han, W.-G.; Jalkanen, K. J.; Elstner, M.; Suhai, S. *J. Phys. Chem. B* **1998**, *102*, 2587.

(45) Drozdov, A. N.; Grossfield, A.; Pappu, R. V. *J. Am. Chem. Soc.* **2004**, *126*, 2574.

(46) Schweitzer-Stenner, R. *J. Raman Spectrosc.* **2001**, *32*, 711.